Taklimakan Desert Nocturnal Low Level Jet: Climatology and Dust Activity

Ge J.M.[1], H.Y. Liu[1, 3], J.P. Huang[1, *], and Q. Fu[1, 2]

[1]Key Laboratory for Semi-Arid Climate Change of the Ministry of Education and College of Atmospheric Sciences, Lanzhou University, Lanzhou, 730000, PRC

[2]Department of Atmospheric Sciences, University of Washington, Seattle, WA, 98105, USA

[3]Hebei Province Meteorological Service Center, Shijiazhuang, 005021, PRC

Submitted to *Atmos. Chem. and Phys.*

hjp@lzu.edu.cn

March 2016

Abstract

While nocturnal Low-Level Jets (NLLJs) occur frequently in many parts of the world, the occurrence and other detailed characteristics of NLLJs over the Taklimakan Desert (TD) are not well known. This paper presents a climatology of NLLJs and coincident dust over the TD by analyzing multi-year ERA-Interim reanalysis and satellite observations. It is found that the ERA-Interim dataset can capture the NLLJs feature well by comparing with radiosonde data from two surface sites. The NLLJs occur in more than 60% of nights, which are primarily easterly to east-northeasterly. They typically appear at 100 to 400 m above the surface with a speed of 4 to 10 ms^{-1}. Most NLLJs are located above the nocturnal inversion during warm season while they are embedded in the inversion layer during cold season. NLLJs above the inversion have a strong annual cycle with a maximum frequency in August. We also quantify the convective boundary layer (CBL) height and construct an index to measure the magnitude of the momentum in the CBL. We find that the NLLJ contains more momentum than without NLLJ, and in warm season the downward momentum transfer process is more intense and rapid. The winds below the NLLJ core to the desert surface gain strength in summer and autumn, which are coincident with an enhancement of aerosol optical depth. It indicates that the NLLJ is an important mechanism for dust activity and transport during the warm season over the Taklimakan.

Key words: Taklimakan Desert, Low-level Jet, Boundary, Dust Aerosol

1. Introduction

The Taklimakan Desert (TD) is one of the largest deserts and located farther from an ocean than any other desert in the world. It occupies the central part of the Tarim Basin in northwestern China, extending about 1000 km from east to west and 400 km from north to south (Figure 1) with a dry continental climate [*Huang et al.*, 2016]. Most of the TD area is composed of shifting sand dunes and it is the most intense dust aerosol source in Asia [*Gao and Washington*, 2009; *Zhang et al.*, 2003]. The TD is of particular interest not only because of its large contribution to the global dust emission [*Uno et al.*, 2009; *Yumimoto et al.*, 2009], but also because of its very unique orography and prevailing winds. The prevailing wind direction in the low level atmosphere of the TD is easterly and northeasterly (Figure 1), which is consistent with the dominant direction of motion of the sand dunes. The elevation of the TD is about 0.8 km above sea level (ASL) at the northeast side of the Tarim basin, increasing gradually to 1.5 km ASL at the southwest area. The basin is open on its eastern side while the other three sides are surrounded by the high relief of mountains and plateaus with an average elevation over 4.5 km. The prevailing northeasterly, low-altitude winds limit the flow of low-level dust out of this region much of the time. However, former studies have indicated that dust from the TD can be lofted above 5 km into the upper troposphere [*Ge et al.*, 2014; *Huang et al.*, 2007], and subsequently transported over long distances and around the globe by the westerlies [*Huang et al.*, 2008; *Uno et al.*, 2009]. This long-lasting dust aerosol can perturb the energy balance of the Earth system through its direct radiative effects on solar and terrestrial radiation [*Fu et al.*, 2009; *Ge et al.*, 2011; 2010; *Huang et al.*, 2014], indirect radiative effects via

its influence on physical properties of clouds [*Huang et al.*, 2014; *Lohmann and Feichter*, 2005; *Su et al.*, 2008], and semi-direct effects by heating the dust layer [*Huang et al.*, 2009; 2014]. Thus, high concentrations of elevated dust and its long range transport from the Taklimakan may play an important role in climate and climate change [*Huang et al.,* 2008; *Ling et al.*, 2014]. To better understand dust emission, transport and the influence on climate will require more exploration of the local and meso-scale meteorological processes over this dust source region.

Dust emission processes are controlled by meteorology and surface properties, such as surface wind, soil texture, moisture content, surface roughness and vegetation[*Ginoux et al.*, 2001; *Knippertz and Todd*, 2012]. A surface wind that exceeds a particle-size-dependent speed threshold is a condition for dust emission [*Shao et al.*, 2011]. Above the threshold the dust emission flux is highly sensitive to wind speed [*Chen et al.*, 2013; *Lu and Shao*, 1999; *Tegen*, 2003]. Synoptic cold fronts are known to lead to strong surface winds, resulting in dust storms over the Taklimakan and Gobi deserts [*Sun et al.*, 2001]. Another mechanism that can lead to strong surface winds in semi-arid and desert regions is through the formation of a Nocturnal Low-Level Jet (NLLJ) [*Fiedler et al.*, 2013; *Rife et al.*, 2010].

NLLJ are generally characterized as a relatively thin layer with highest wind speeds in a core between 300 and 600 meters above ground level (AGL) while there are usually minima in wind speed 1.0 to 2.0 km above the core [*Rife et al., 2010*]. A diurnal cycle is a common and well documented feature of NLLJ with onset and cessation times generally in the early evening and mid-morning, respectively.

Maximum speeds occur around 0000 to 0300 local time. Nocturnal low-level jets with diurnal variability form primarily by two mechanisms. One mechanism is the forcing by changes in baroclinicity associated with orographic channeling, temperature gradients over sloping terrain, coastal area and across weather front [*Baas et al.*, 2009; *Stensrud*, 1996; *Washington and Todd*, 2005]. The other is related to the decoupling of winds from the surface friction, and subsequent recoupling due to diurnally varying eddy viscosity. This is the initial oscillation mechanism (IO) as advanced by [*Blackadar*, 1957; *Van de Wiel et al.*, 2010]. The formation of NLLJs is favored over relatively flat terrain in arid and semi-arid regions. When these essentially local forcing mechanisms exist on a large scale over relatively uniform, level terrain such as the Taklimakan, the NLLJ can extend to the meso and synoptic scales and may couple to mid-tropospheric winds thus promoting long-range transport of dust particles. A remarkable feature of the NLLJ is its breakdown after sunrise when the NLLJ momentum is mixed to the surface, and thus wind speed near the surface is greatly increased [*Fiedler et al.*, 2013; *Schepanski et al.*, 2009]. The strong surface wind will blow up dust particles from the desert surface and the same turbulent mixing will also loft these dust to the upper level of the boundary layer, promoting horizontal transport. Therefore, the NLLJ may play an important role in the both dust emission and transport [*Allen and Washington*, 2014; *Heinold et al.*, 2015; *Knippertz*, 2008; *Tegen et al.*, 2013; *Todd et al.*, 2008].

Much work has been done to address the features of the NLLJ, demonstrating a link between NLLJs and dust suspension and their contribution to dust emission over

northern Africa [*Allen and Washington*, 2014; *Fiedler et al.*, 2013; *Schepanski et al.*, 2009; *Washington and Todd*, 2005]. Since the TD has a hyper-arid environment and relative flat terrain, strong radiative cooling during the night in this region can stabilize the near surface layer and at least partly decouple the air from the surface layer friction that will provide a favorable condition for NLLJ formation. We anticipate that the frictional decoupling after sunset with a subsequent inertial oscillation may play an important role in the formation of NLLJ for this area. However, there have been very few NLLJ studies over the Taklimakan region. Rife et al.[2010] examined the Tarim basin NLLJ, but only focused on its diurnal variation for July. Du et al. [2014] simulated diurnal variations of Tarim basin NLLJs during early summer from 2006 to 2011 by using the Weather Research Forecast (WRF) model. In this paper, we present an NLLJ detection algorithm and show the climatology and seasonal variation of NLLJ over the Taklimakan by using the ERA-Interim reanalysis data. Satellite-based aerosol optical depth (AOD) above the Taklimakan is also analyzed to explore the effect of this NLLJ on dust emission from the desert surface.

2. Data

The essential data for the characterization of NLLJs over the TD is the latest global atmospheric reanalysis fields of the ERA-Interim data on the model levels. It is produced by European Centre for Medium-Range Weather Forecasts (ECMWF) covering the data-rich period since 1979 and continuing in real time. Comparing with the previous reanalysis data from ECMWF, the ERA-Interim has many substantial

132 improvements on the representation of the hydrological cycle, the quality of the
133 stratospheric circulation, and the handling of biases and changes in the observing
134 system [*Dee et al.*, 2011]. The horizontal resolution of the data set is about 80 km
135 with 60 vertical levels from the surface up to 0.1 hPa. The 6-hourly daily wind speeds
136 and temperatures with a spatial resolution of $1^{\circ} \times 1^{\circ}$ from 2000 to 2013 were analyzed
137 in this study. We choose the ERA-Interim reanalysis for the climatological study of
138 NLLJs, because surface observations are very sparse due to the remoteness and harsh
139 environment of the TD and the ERA-Interim can provide sufficient vertical resolution.
140 Radiosonde data from two surface sites, Korla (86.08ºE, 41.45ºN) and Ruoqiang
141 (88.10ºE, 39.02ºN) (see Figure 1), were also used in this study. The radiosondes at
142 these two sites are launched at 08 and 20 Beijing time (BJT, eight hours ahead of
143 UTC) and have been operating more than 50 years. The quality controlled dataset is
144 updated through 2012. We compared ERA-Interim horizontal wind speed with
145 soundings at 00 UTC to validate reanalysis data.
146 The Multi-angle Imaging Spectro-Radiometer (MISR) onboard the Terra satellite,
147 which crosses the equator at 10:30 AM in its descending node, covers a swath of
148 approximately 360 km wide at the Earth's surface and obtains global coverage in
149 about 9 days. By taking advantage of the nine widely-spaced angles, MISR can
150 distinguish the top-of-atmosphere (TOA) reflectance contributions from the surface
151 and atmosphere, and successfully retrieve aerosol optical properties over bright
152 surfaces [*Diner et al.*, 2005]. In this study, we used level 3 daily AOD from 2000
153 through 2013 at 0.5° by 0.5° resolution to obtain the climatology of AOD and its

154 monthly variation over the Taklimakan.

155 **3. Detection of NLLJs**

156 The mean annual cycle of MISR-based AOD and ERA-Interim wind speed at 10 m
157 above surface, averaged over the TD region (see white box in Figure 1) for 2000-2013,
158 are shown in Figure 2. It is obvious that dust loading over the TD has a clear seasonal
159 variation. The AOD peaks in April and May with a monthly median value of ~0.5
160 while it decreases to a minimum in November and December with a monthly median
161 value of ~0.2. We can also see that the AOD at 95 percentile for the month with
162 minimum median value can exceed 0.7, demonstrating that a large amount of dust can
163 be emitted over the TD throughout the year. The generation of dust aerosol, as well as
164 the consequent particle concentration, is highly dependent on the surface wind speed.
165 A study by Ge et al. [2014] has indicated a strong relationship between AOD and near
166 surface wind over this region. Figure 2 clearly shows that the monthly median value
167 of winds has the same trend as the AOD. Similar to the large spread of AOD, the
168 wind speed also has a wide range in each month.

169 Note that the annual mean circulation at 850 hPa (Figure 1) shows a band of high
170 wind speeds in the central Taklimakan. Figure 3 shows the vertical-latitudinal
171 distribution of annual mean wind speeds at 00 UTC (0600 local time) for the
172 longitudes of 82^{o}, 85^{o} and 88^{o}E. It reveals that there is a maximum wind core centered
173 near 40^{o}N at about 300-400 m AGL with a wind speed exceeding of 6.5 ms^{-1}. It can
174 extend over 10^{o} in longitude and over 1^{o} in latitude. Such night-time jet core occurs
175 widely and frequently over the TD. This phenomenon motivates us to examine the

176 details and climatology of NLLJs over the TD region and investigate the potential
177 effects of NLLJs on dust emission.

178 Before we use the ERA-Interim dataset to characterize the mesoscale episodes of
179 NLLJs occurring over the TD, it is necessary to validate the reanalysis data first. We
180 compared radiosonde data at the Ruoqiang and Korla sites with ERA-Interim winds at
181 the grids nearest to the observations sites during 2000 through 2012 when both the
182 reanalysis and validated sounding data are available. Figure 4 shows the comparison
183 of mean vertical wind speed profiles from reanalysis to a 13-year subset of sounding
184 data. We can see that the representation of the vertical wind structure in ERA-Interim
185 is reasonably good as compared with radiosondes. Importantly, the reanalysis data can
186 reasonably well approximate the height of the maximum low level winds, although
187 ERA-Interim underestimates the NLLJ winds at Ruoqiang, but overestimates them at
188 Korla. We also compared the time series of wind speeds from reanalysis and
189 radiosondes at 100 and 600 m AGL (not shown), and calculated the correlation
190 coefficients and Root Mean Square Errors (RMSE). Ruoqiang has a higher correlation
191 coefficient that is 0.51 for the layer of 600 m AGL, while the RMSE of 4.9 ms^{-1} at
192 Korla is about 0.5 ms^{-1} smaller than that at Ruoqing. Thus, we may expect that the
193 ERA-Interim adequately represents the wind structures over the TD.

194 In order to investigate the climatology of NLLJs over the TD, a set of objective
195 criteria for automatically identifying their occurrences need to be specified. In the
196 literature, many criteria have been applied for identifying LLJs associated with
197 different formation mechanisms, data sets used and definitions of LLJ [*Bonner,* 1968;

198 *Stull,* 1988; *Banta et al.,* 2002; *Baas et al.,* 2009]. They include the range of
199 maximum wind height, threshold of wind speed at the jet core, and strength of vertical
200 wind shear. Here we developed an algorithm to detect the NLLJs from the
201 ERA-Interim reanalysis data by partly following the criteria given in Fiedler et al.
202 [2013] and Ranjha et al. [2013] where the ERA-Interim reanalysis data were used to
203 identify LLJs. First, a temperature inversion condition is identified and the inversion
204 top height (H_i) is determined by scanning each temperature profile by following the
205 protocol proposed by Kahl [1990]. H_i must be above the third model level, i.e.
206 roughly 60 m (agl). This criterion generally assures that the lowest atmospheric layers
207 are stable and that the surface frictional drag on the air flowing above it is reduced.
208 Second, the maximum wind speed below 1500 m agl and its height (H_j) are
209 determined. The jet heights are confined to less than 1500 m following Fiedler et
210 al.[2013]. However, reducing this criterion to 900 m decreases the NLLJ occurrence
211 frequency by only 1 percent. Third, a wind speed minimum must exist above the
212 NLLJ but below 5 km agl with a value 60% or less relative to the wind speed of the
213 jet core. This condition is a combination and simplification of the second and third
214 criteria proposed by Ranjha et al. [2013], which is a description of LLJ wind shear
215 and ensures that identified NLLJs always have jet-like profiles.

216 **4. Climatology of NLLJs**

217 By applying these criteria to the 14-year ERA-Interim data, we found that the NLLJ
218 commonly appears over the Taklimakan and other adjacent arid regions. Figure 5
219 shows the monthly mean frequency of NLLJs for the TD and surrounding areas along

220 with contours of jet core speed. It is interesting to note that the NLLJs occurrence
221 frequency distribution derived from this identification method is closely related to the
222 topography and land surface type. One can see that the main feature of Figure 5 is a
223 frequency mode with values greater than 60% appearing in the entire Tarim Basin
224 throughout the year. The geographical distribution of NLLJs can extend eastward
225 from the main mode over the TD to the Loss Plateau along the north slope of the
226 Tibetan Plateau with decreasing frequency of occurrence toward the east. There are
227 also two other high frequency modes located near the TD region. One is in the Jungar
228 Basin located in northern Xinjiang which is a semi-arid area. The other is over desert
229 centered at 76^{o}E, 46^{o}N in Kazakhstan. It is also obvious that there is rough co-location
230 of maxima in NLLJ wind speed and frequency. Figure 5 indicates that the jet
231 detection algorithm is successful. The NLLJ is a frequent mesoscale weather
232 phenomenon over the TD and adjacent desert basins.

233 Figure 6 shows the climatological statistics of (a) jet height, (b) core speed, (c)
234 seasonal variation and (d) jet direction. Typically, the NLLJ occurs in a very shallow
235 layer. About 67% of the jet cores are located between 120 and 400 m AGL. 75% of
236 the jet core speeds fall between 4 and 10 ms^{-1}. The median values of the jet height and
237 jet core speed are 269 m and 6 ms^{-1}, respectively. By comparison, the median values
238 of the NLLJ height and core speed derived from ERA-Interim data for North Africa
239 [*Fiedler et al.*, 2013] are at 350 m and 10 ms^{-1}, which are higher and greater than
240 those over the Taklimakan, respectively. Figure 6c illustrates the monthly
241 climatology of jet height, jet core maximum speed and inversion height. We can see

242 that all these three parameters have clear seasonal variations. The jet speed generally
243 follows the trend of jet height that increases gradually from cold season to warm
244 season and has a maximum in August. The tendency for stronger NLLJs to occur at
245 higher levels is the same as those found in other places [*Banta et al.,* 2002; *Baas et al.,*
246 2009; *Fiedler et al.,* 2013]. According to Blackadar's classical theory of IO
247 [*Blackadar,* 1957], the nocturnal inversion plays an important role in reducing eddy
248 viscosity and decoupling the air aloft in the planetary boundary layer from the surface
249 boundary layer. It thus causes a frictionless layer at the top of the inversion which is
250 the initial condition for the formation of NLLJ. However, we note that the jet can be
251 found at different heights which could be above the inversion top or embedded in the
252 inversion layer [*Andreas et al.*, 2000; *Baas et al.*, 2009]. Figure 6c shows that the
253 inversion height has an opposite seasonal trend to that of jet height. The inversion
254 height has minimum values in summer season, and can be as thick as 600 m in later
255 fall and winter which is much higher than the jet height of about 230 m. Our analysis
256 indicates that about half of the identified NLLJ cores are above the top of inversion
257 and the other half were embedded or partially embedded in the inversion layer. The
258 low solar elevation angle and high desert surface reflectivity during the cold season
259 would result in less sensible heat and thus a shallower day-time boundary layer but a
260 thicker nocturnal inversion layer. In these cases the NLLJ occurs a few hundred
261 meters above the surface where the layer is well stratified after sunset.

262 The wind rose in figure 6d shows that the prevailing wind direction of the jet core
263 is narrowly distributed between east-northeast and east-southeast, 67 percent of

NLLJs over all seasons are within the four sectors between 40 and 120 degrees. This narrow angular NLLJ directional distribution is mainly confined by the topography.

5. NLLJ effects on dust emission

Considering that the emission of dust initially develops in the surface boundary layer and is proportional to third or fourth power of the surface wind speed, it is expected that the NLLJ can affect dust production if we can find that NLLJ do have impacts on near surface wind speed and variability. Recent studies [*Christopher & Washington,* 2014; *Heinold et al*., 2013; *Knippertz,* 2008; *Schepanski et al.,* 2009] have indicated that the breakdown of the NLLJ over Africa can induce the downward mixing of momentum during the evolution of the boundary layer in mid-morning and cause enhancement of near surface wind speed. Here, we firstly compared the mid-morning surface wind speed distribution coincident with the appearance of NLLJ with that when no NLLJ was detected. Ideally this would have been calculated for 10:00 AM local time to observe the maximum effect but only 6-hourly ERA data were available. Figure 7 shows the near surface wind speed frequency distribution at 06 UTC (i.e., 11:30 AM local time) over the Taklimakan. We can see an obvious shift of wind speed toward higher values when NLLJs are present compared to the days when there is no NLLJ. This result may be an evidence of NLLJ effects on surface wind speed and a link between NLLJs and dust emission. However, if we take a further look at the detailed behavior of near surface wind speed difference between jet and non-jet days for the seasonal cycle over the Tarim basin, the spatial distributions of wind speed difference of each month are substantially different. In Figure 8, we can

see that positive differences are dominant in the basin during cold season from October to March, but negative values are distributed over the most basin area with only a weak positive belt aligning along the north slope of the Tibet Plateau during April to September. This seasonal contrast in the surface wind speed difference is exactly coincident with the relative position of jet height and inversion height that are shown in Figure 6c. As we know, a convective boundary layer starts with morning insolation, grows gradually to dissipate the nocturnal surface inversion and transport momentum from aloft to the surface. However, this process could be either very rapid or much slower depending on solar heating and other meteorological conditions. We may expect when the inversion layer is much thicker and the surface heating is very weak in the cold season, the development of mixed layer may be very slow and the unstable layer happens to reach the height of NLLJ at 06 UTC. Thus momentum from the LLJ is mixed down and leads to an increase of the surface wind speed, showing a positive difference during these months. By contrast in the warm season, a mixed boundary layer is developed very rapidly, LLJ momentum transport process may have been already largely completed by 06 UTC. The surface friction is well coupled with boundary layer and consumes the downward momentum, eventually leads to a sub-geostrophic wind.

To test this hypothesis, we need to further investigate the height of convective boundary layer (CBL) in the mid-morning (06 UTC). The Richardson number (Ri) [*Richardson et al.*, 2013] that indicates the dynamic instability of the flow is used here to determine the CBL height. The Ri is a measure of relative strength of

buoyance and mechanical wind shear. It is defined as:

$$R_i = \frac{\frac{g}{\theta}\left(\frac{\partial \theta}{\partial z}\right)}{\left(\frac{\partial u}{\partial z}\right)^2 + \left(\frac{\partial v}{\partial z}\right)^2}$$

where θ is the potential temperature, g is the acceleration of gravity, z is the height, and u and v are the horizontal wind velocity components. Clearly, turbulent energy increases when Ri < 1, but theoretical and experimental studies show that non-turbulent flow becomes turbulent when Ri drops below a critical value of around 0.25. We first selected those profiles in which the potential temperature at the lowest level is larger than at the next higher level to ensure that the turbulence is induced by surface heating. Then we calculated the Ri numbers between successive levels for the selected profiles, and searched each profile from the surface upwards, and defined the lowest level, where Ri value exceeds the critical value of 0.25, as the top of the CBL. The red lines in Figure 9 plot the monthly variations of the CBL height at 06 UTC averaged on days with and without NLLJ over the TD. The variations for both jet and no jet cases exhibit the same tendency that the greatest heights appear in June and the lowest heights of about 200 m occur in December and January. Obviously, the tendencies are primarily a response to the solar insolation which is the primary control of near-surface heating. During cold season from October to March, the monthly mean CBL heights on jet days are almost the same as those on no jet days, and close to the jet core height. Significant differences in CBL heights between jet and non-jet days are evident in the months from April to September. We examined the occurrence of clouds and total cloud cover (TCC) derived from ERA-Interim data, and found that

both the occurrence of clouds and TCC on NLLJ days are much smaller than no-jet days. It is clear that less clouds can let more thermal radiation escape to space and allow intensive radiative cooling to form a stable surface layer during night, leading to the development of NLLJ aloft. In midmorning, less clouds also allow more solar radiation to reach at the surface and thus cause a stronger surface heating that consequently induces a stronger turbulence and a higher mixed layer than non-jet days. We may infer that stronger vertical mixing on days with jet occurrence can transport momentum between the surface and a given height in or above the stable layer rapidly in the warm season.

Having quantified the CBL height, we next quantified the magnitude of the momentum in the boundary by constructing an index. It is a summation of wind speed from the height just above the surface layer to the height of the CBL with a unit of m^2s^{-1}:

$$\text{Index} = \int_{H_s}^{H_c} U(h)dh$$

where H_s is the top of the surface layer which is typically about 10% of the boundary layer depth which we selected as the height of the third model level above the surface. H_c is the top of the CBL that is derived from Ri and U(h) is the wind speed profile. We applied this index on each grid of the ERA-Interim at 00 UTC and averaged the index values over the TD region. The blue lines in Figure 9 show the monthly variations of the momentum index for days with and without NLLJ occurring at 00 UTC. The seasonal trends of the index are largely determined by the integral depth (i.e. the height of the CBL) and thus vary consistently with the CBL height. More

351 importantly, the momentum index on days with NLLJs are always larger than those on
352 days without NLLJs even if there is not a big difference in H_c between jet and non-jet
353 cases. Note that for both NLLJ and non-NLLJ cases CBL heights during October
354 through March are almost the same but are significantly different during the warm
355 season. By combining the CBL height, momentum index and near surface wind speed
356 shown in Figure 8 and 9, we may draw a conclusion that at night the boundary layer
357 between H_s and H_c with NLLJ contains more momentum than without NLLJ. When
358 the NLLJ breaks down in midmorning its momentum is transported toward the
359 surface, decreasing the speed aloft but producing stronger surface winds. During cold
360 season, the inversion depth is greater and vertical mixing is weaker that consequently
361 result in less downward momentum transfer that occurs over a longer period of time.
362 In the summer season, the downward momentum transfer process is more intense and
363 rapid and could cause a significant increase in surface wind speed which is not
364 captured by the 6-hour ERA dataset.

365 The above investigation has indicated that the momentum in an upper boundary
366 layer is larger, and the turbulence is much stronger especially in summer for the NLLJ
367 cases than without NLLJ occurrence. A larger momentum and stronger transfer
368 consequently can lead to an enhancement of the surface wind speed. In order to
369 explore a link between NLLJs and dust activity, a composite difference method is
370 used to analyze the relationship between NLLJ winds and dust generation. We point
371 out that if the wind profile composite is simply based on high and low dust loading,
372 an enhancement of wind in the lower atmosphere will always be seen because larger

373 wind speed is directly related to dust generation for a given surface condition. Thus,
374 there is a risk of evaluating the effect of NLLJ on dust emission since we cannot tell if
375 stronger surface winds are associated with the NLLJ. To avoid this risk, we select
376 only ERA-Interim data for which 80% of the grid points along the section at 40º N
377 between the latitudes of 78 and 88º E are identified with the appearance of NLLJ. We
378 then match the time series of the NLLJ data and AOD observations for the composite
379 analysis. According to the seasonal distribution of AOD, we use the 10 and 90
380 percentile values of the AOD cumulative distribution function to identify the most and
381 least dusty days and 42 samples for winter and 58 samples for each of the other three
382 seasons are picked out for the composite difference analysis. Figure 10 shows the
383 seasonal composite differences of latitudinal wind speed between the most and least
384 dusty days along 40º N. It is clear that the NLLJ is significantly enhanced on days of
385 high AOD for summer and autumn seasons and that the core speed increases by more
386 than 3 ms^{-1}. Due to stronger turbulent mixing in summer compared to other seasons,
387 NLLJ level winds may affect the surface wind speed and variance causing a deeper
388 surface layer with a significant increase of wind speed on high dust days in summer
389 than autumn.

390 We also notice an interesting phenomenon that although AOD values are highest
391 in spring (Figure 2), NLLJ speeds are not significantly higher in this season. It is well
392 known that cold frontal with high synoptic scale winds cause strong dust storms in
393 spring[*Sun et al.*, 2001]. Obviously our results indicate that occurrences of NLLJ have
394 relatively less influence on dust emission in the spring when synoptic scale winds

dominate dust emission.

6. Conclusion

In this study, we presented a long-term, detailed structure of the wind profile in the atmospheric boundary layer over the Taklimakan Desert which has a relative flat terrain. A comparison of radiosondes and ERA-Interim reanalysis at two sites in the Tarim basin shows that the reanalysis data can capture the feature of the low level wind profile. Based on our NLLJ detection algorithm, NLLJs are frequent over the entire Tarim Basin and Taklimakan Desert throughout the entire year with an occurrence frequency above 60%. The dominant wind directions are east and east-northeast in all seasons. The annual mean values of jet height and core speed are 270 m and 6 ms^{-1}, respectively. The jet core height and speed show seasonal variations, both with maximum values in August and minimum in January. The inversion height also changes with season, but in a manner opposite to the height of the jet core. We found that about 50% of the identified NLLJ cores are above the top of inversion (more frequently in the warmer season), and the other half of NLLJs was embedded in the inversion layer (mostly in the colder season).

The midmorning breakdown of the nocturnal inversion and jet core are remarkable and consistent features of NLLJ over the TD. The momentum of these NLLJ can be mixed downward, increasing surface wind speed, which could be the driving mechanism for dust emission over this and other arid regions. We calculated the CBL height, and constructed an index to quantify the magnitude of the momentum from the top of the surface layer to the CBL height. It is found that the momentum in an upper

boundary layer is larger for the NLLJ cases than without NLLJ occurrence in all seasons, while the CBL heights in warm season are much greater than those in cold season. This indicates that stronger vertical mixing on days with jet occurrence can transport more momentum between the surface and CBL height in the warm season, thus enhancing the surface wind speed.

We further matched the NLLJ and MISR AOD data and found that there was a significant enhancement of NLLJ during high AOD days in summer and autumn seasons when the core speed increased by more than 3 ms^{-1}. In the cold season, the sensible heat energy input is much less and the inversion layer is thicker which cause much weaker downward propagation of turbulence, thus NLLJs have a lesser effect on surface wind and dust activity in winter and spring.

Nocturnal low-level jets have been identified as a frequent mesoscale phenomenon over the TD and are possibly an important mechanism for dust activity especially in the summer months. To define the details of the NLLJ diurnal cycle and to clarify the causal and quantitative relationships to dust emission and transport, further ground-based in-situ and remote sensing measurements of winds and dust concentration profiles are needed along with high spatial and temporal resolution numerical modeling.

Data availability: The data for this paper are available at NASA Atmospheric Data Center and ECMWF. Data sets: MISR, ERA Interim. Date name: MIL3DAE_*.004_*.hdf, ERA_Interim_*.nc

Acknowledgements: This work was supported by the National Science Foundation of China (41275070, 41521004, 41575016), China 111 project (No.B 13045), and the Fundamental Research Funds for the Central University (lzujbky-2015-K02). We

thank Prof. Dave S. Covert for useful comments and discussion.

443 References

444 Allen, C. J. T., and R. Washington (2014), The low-level jet dust emission mechanism
445 in the central Sahara: Observations from Bordj-Badji Mokhtar during the June 2011
446 Fennec Intensive Observation Period, *Journal of Geophysical Research-Atmospheres*,
447 *119*(6), 2990-3015, doi:10.1002/2013jd020594.

448 Andreas, E. L., K. J. Claffy, and A. P. Makshtas (2000), Low-level atmospheric jets
449 and inversions over the western Weddell Sea, *Boundary-Layer Meteorology*, *97*(3),
450 459-486, doi:10.1023/a:1002793831076.

451 Baas, P., F. C. Bosveld, H. K. Baltink, and A. A. M. Holtslag (2009), A Climatology
452 of Nocturnal Low-Level Jets at Cabauw, *Journal of Applied Meteorology and*
453 *Climatology*, *48*(8), 1627-1642, doi:10.1175/2009jamc1965.1.

454 Blackadar, A. K. (1957), Boundary layer wind maxima and their significance for the
455 growth of nocturnal inversions, edited, pp. 283-290, Bulletin of the American
456 Meteorological Society.

457 Chen, S., J. Huang, C. Zhao, Y. Qian, L. R. Leung, and B. Yang (2013), Modeling the
458 transport and radiative forcing of Taklimakan dust over the Tibetan Plateau: A case
459 study in the summer of 2006, *Journal of Geophysical Research-Atmospheres*, *118*(2),
460 797-812, doi:10.1002/jgrd.50122.

461 Dee, D. P., et al. (2011), The ERA-Interim reanalysis: configuration and performance
462 of the data assimilation system, *Quarterly Journal of the Royal Meteorological*
463 *Society*, *137*(656), 553-597, doi:10.1002/qj.828.

464 Diner, D. J., J. V. Martonchik, R. A. Kahn, B. Pinty, N. Gobron, D. L. Nelson, and B.
465 N. Holben (2005), Using angular and spectral shape similarity constraints to improve

MISR aerosol and surface retrievals over land, *Remote Sensing of Environment*, *94*(2), 155-171, doi:10.1016/j.res.2004.09.009.

Fiedler, S., K. Schepanski, B. Heinold, P. Knippertz, and I. Tegen (2013), Climatology of nocturnal low-level jets over North Africa and implications for modeling mineral dust emission, *Journal of Geophysical Research-Atmospheres*, *118*(12), 6100-6121, doi:10.1002/jgrd.50394.

Fu, Q., T. J. Thorsen, J. Su, J. M. Ge, and J. P. Huang (2009), Test of Mie-based single-scattering properties of non-spherical dust aerosols in radiative flux calculations, *Journal of Quantitative Spectroscopy & Radiative Transfer*, *110*(14-16), 1640-1653, doi:10.1016/j.jqsrt.2009.03.010.

Gao, H., and R. Washington (2009), The spatial and temporal characteristics of TOMS AI over the Tarim Basin, China, *Atmospheric Environment*, *43*(5), 1106-1115, doi:10.1016/j.atmosenv.2008.11.013.

Ge, J. M., J. P. Huang, J. Su, J. R. Bi, and Q. Fu (2011), Shortwave radiative closure experiment and direct forcing of dust aerosol over northwestern China, *Geophysical Research Letters*, *38*, doi:10.1029/2011gl049571.

Ge, J. M., J. P. Huang, C. P. Xu, Y. L. Qi, and H. Y. Liu (2014), Characteristics of Taklimakan dust emission and distribution: A satellite and reanalysis field perspective, *Journal of Geophysical Research-Atmospheres*, *119*(20), 11772-11783, doi:10.1002/2014jd022280.

Ge, J. M., J. Su, T. P. Ackerman, Q. Fu, J. P. Huang, and J. S. Shi (2010), Dust aerosol optical properties retrieval and radiative forcing over northwestern China during the

2008 China-US joint field experiment, *Journal of Geophysical Research-Atmospheres*, *115*, doi:10.1029/2009jd013263.

Ginoux, P., M. Chin, I. Tegen, J. M. Prospero, B. Holben, O. Dubovik, and S. J. Lin (2001), Sources and distributions of dust aerosols simulated with the GOCART model, *Journal of Geophysical Research-Atmospheres*, *106*(D17), 20255-20273, doi:10.1029/2000jd000053.

Heinold, B., P. Knippertz, and R. J. Beare (2015), Idealized large-eddy simulations of nocturnal low-level jets over subtropical desert regions and implications for dust-generating winds, *Quarterly Journal of the Royal Meteorological Society*, *141*(690), 1740-1752, doi:10.1002/qj.2475.

Huang, Q. Fu, J. Su, Q. Tang, P. Minnis, Y. Hu, Y. Yi, and Q. Zhao (2009), Taklimakan dust aerosol radiative heating derived from CALIPSO observations using the Fu-Liou radiation model with CERES constraints, *Atmospheric Chemistry and Physics*, *9*(12), 4011-4021.

Huang, P. Minnis, B. Chen, Z. Huang, Z. Liu, Q. Zhao, Y. Yi, and J. K. Ayers (2008), Long-range transport and vertical structure of Asian dust from CALIPSO and surface measurements during PACDEX, *Journal of Geophysical Research-Atmospheres*, *113*(D23), doi:10.1029/2008jd010620.

Huang, P. Minnis, Y. Yi, Q. Tang, X. Wang, Y. Hu, Z. Liu, K. Ayers, C. Trepte, and D. Winker (2007), Summer dust aerosols detected from CALIPSO over the Tibetan Plateau, *Geophysical Research Letters*, *34*(18), doi:10.1029/2007gl029938.

Huang, T. Wang, W. Wang, Z. Li, and H. Yan (2014), Climate effects of dust aerosols

510 over East Asian arid and semiarid regions, *Journal of Geophysical*
511 *Research-Atmospheres*, *119*(19), 11398-11416, doi:10.1002/2014jd021796.
512 Huang, H. Yu, X. Guan, G. Wang, and R. Guo (2016), Accelerated dryland expansion
513 under climate change, *Nature Climate Change*, *6*(2), 166-+,
514 doi:10.1038/nclimate2837.
515 Kahl, J. D. (1990), CHARACTERISTICS OF THE LOW-LEVEL TEMPERATURE
516 INVERSION ALONG THE ALASKAN ARCTIC COAST, *International Journal of*
517 *Climatology*, *10*(5), 537-548, doi:10.1002/joc.3370100509.
518 Knippertz, P. (2008), Dust emissions in the West African heat trough - the role of the
519 diurnal cycle and of extratropical disturbances, *Meteorologische Zeitschrift*, *17*(5),
520 553-563, doi:10.1127/0941-2948/2008/0315.
521 Knippertz, P., and M. C. Todd (2012), MINERAL DUST AEROSOLS OVER THE
522 SAHARA: METEOROLOGICAL CONTROLS ON EMISSION AND TRANSPORT
523 AND IMPLICATIONS FOR MODELING, *Reviews of Geophysics*, *50*,
524 doi:10.1029/2011rg000362.
525 Lohmann, U., and J. Feichter (2005), Global indirect aerosol effects: a review,
526 *Atmospheric Chemistry and Physics*, *5*, 715-737.
527 Lu, H., and Y. P. Shao (1999), A new model for dust emission by saltation
528 bombardment, *Journal of Geophysical Research-Atmospheres*, *104*(D14),
529 16827-16841, doi:10.1029/1999jd900169.
530 Richardson, H., S. Basu, and A. A. M. Holtslag (2013), Improving Stable
531 Boundary-Layer Height Estimation Using a Stability-Dependent Critical Bulk

532 Richardson Number, *Boundary-Layer Meteorology*, *148*(1), 93-109,
533 doi:10.1007/s10546-013-9812-3.
534 Rife, D. L., J. O. Pinto, A. J. Monaghan, C. A. Davis, and J. R. Hannan (2010), Global
535 Distribution and Characteristics of Diurnally Varying Low-Level Jets, *Journal of*
536 *Climate*, *23*(19), 5041-5064, doi:10.1175/2010jcli3514.1.
537 Schepanski, K., I. Tegen, M. C. Todd, B. Heinold, G. Boenisch, B. Laurent, and A.
538 Macke (2009), Meteorological processes forcing Saharan dust emission inferred from
539 MSG-SEVIRI observations of subdaily dust source activation and numerical models,
540 *Journal of Geophysical Research-Atmospheres*, *114*, doi:10.1029/2008jd010325.
541 Shao, Y., K.-H. Wyrwoll, A. Chappell, J. Huang, Z. Lin, G. H. McTainsh, M. Mikami,
542 T. Y. Tanaka, X. Wang, and S. Yoon (2011), Dust cycle: An emerging core theme in
543 Earth system science, *Aeolian Research*, *2*(4), 181-204,
544 doi:10.1016/j.aeolia.2011.02.001.
545 Stensrud, D. J. (1996), Importance of low-level jets to climate: A review, *Journal of*
546 *Climate*, *9*(8), 1698-1711, doi:10.1175/1520-0442(1996)009<1698:iolljt>2.0.co;2.
547 Su, J., J. Huang, Q. Fu, P. Minnis, J. Ge, and J. Bi (2008), Estimation of Asian dust
548 aerosol effect on cloud radiation forcing using Fu-Liou radiative model and CERES
549 measurements, *Atmospheric Chemistry and Physics*, *8*(10), 2763-2771.
550 Sun, J. M., M. Y. Zhang, and T. S. Liu (2001), Spatial and temporal characteristics of
551 dust storms in China and its surrounding regions, 1960-1999: Relations to source area
552 and climate, *Journal of Geophysical Research-Atmospheres*, *106*(D10), 10325-10333,
553 doi:10.1029/2000jd900665.

554 Tegen, I. (2003), Modeling the mineral dust aerosol cycle in the climate system,
555 *Quaternary Science Reviews*, *22*(18-19), 1821-1834,
556 doi:10.1016/s0277-3791(03)00163-x.
557 Tegen, I., K. Schepanski, and B. Heinold (2013), Comparing two years of Saharan
558 dust source activation obtained by regional modelling and satellite observations,
559 *Atmospheric Chemistry and Physics*, *13*(5), 2381-2390,
560 doi:10.5194/acp-13-2381-2013.
561 Todd, M. C., R. Washington, S. Raghavan, G. Lizcano, and P. Knippertz (2008),
562 Regional model simulations of the Bodele low-level jet of northern Chad during the
563 Bodele Dust Experiment (BoDEx 2005), *Journal of Climate*, *21*(5), 995-1012,
564 doi:10.1175/2007jcli1766.1.
565 Uno, I., K. Eguchi, K. Yumimoto, T. Takemura, A. Shimizu, M. Uematsu, Z. Liu, Z.
566 Wang, Y. Hara, and N. Sugimoto (2009), Asian dust transported one full circuit
567 around the globe, *Nature Geoscience*, *2*(8), 557-560, doi:10.1038/ngeo583.
568 Van de Wiel, B. J. H., A. F. Moene, G. J. Steeneveld, P. Baas, F. C. Bosveld, and A. A.
569 M. Holtslag (2010), A Conceptual View on Inertial Oscillations and Nocturnal
570 Low-Level Jets, *Journal of the Atmospheric Sciences*, *67*(8), 2679-2689,
571 doi:10.1175/2010jas3289.1.
572 Washington, R., and M. C. Todd (2005), Atmospheric controls on mineral dust
573 emission from the Bodele Depression, Chad: The role of the low level jet,
574 *Geophysical Research Letters*, *32*(17), doi:10.1029/2005gl023597.
575 Yumimoto, K., K. Eguchi, I. Uno, T. Takemura, Z. Liu, A. Shimizu, and N. Sugimoto

576 (2009), An elevated large-scale dust veil from the Taklimakan Desert: Intercontinental
577 transport and three-dimensional structure as captured by CALIPSO and regional and
578 global models, *Atmospheric Chemistry and Physics*, *9*(21), 8545-8558.
579 Zhang, X. Y., S. L. Gong, T. L. Zhao, R. Arimoto, Y. Q. Wang, and Z. J. Zhou (2003),
580 Sources of Asian dust and role of climate change versus desertification in Asian dust
581 emission, *Geophysical Research Letters*, *30*(24), doi:10.1029/2003gl018206.
582

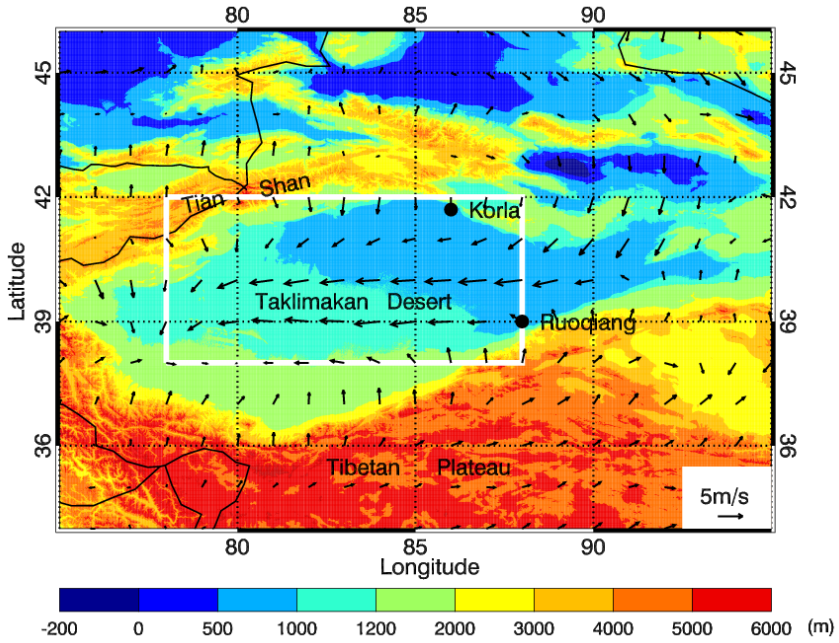

583

584 Figure 1. Map of the Taklimakan Desert region with its topography and annual mean

585 wind at 850 hPa.

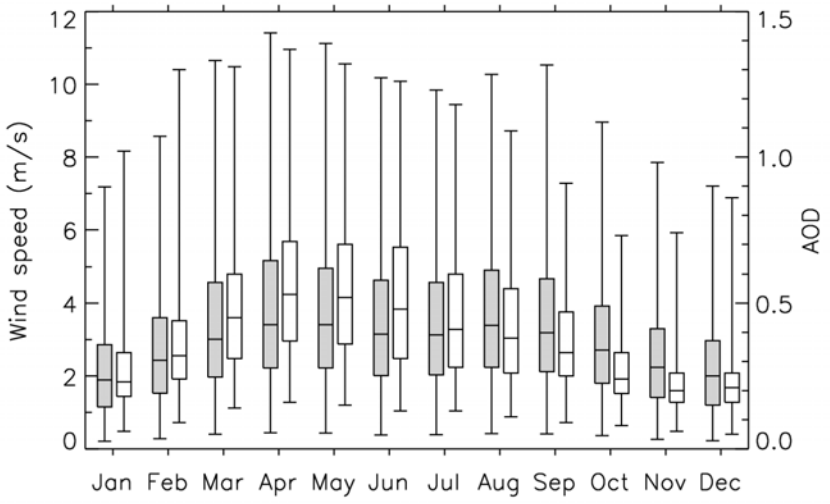

586

587 Figure 2. Annual cycles of wind speed (gray bars) and AOD (white bars) from 2000

588 through 2013 over the Taklimakan Desert. The horizontal line through each box

589 represents that monthly median value; top and bottom of the boxes mark 75% and 25%

590 percentiles, respectively; whiskers mark the 95% and 5% percentiles.

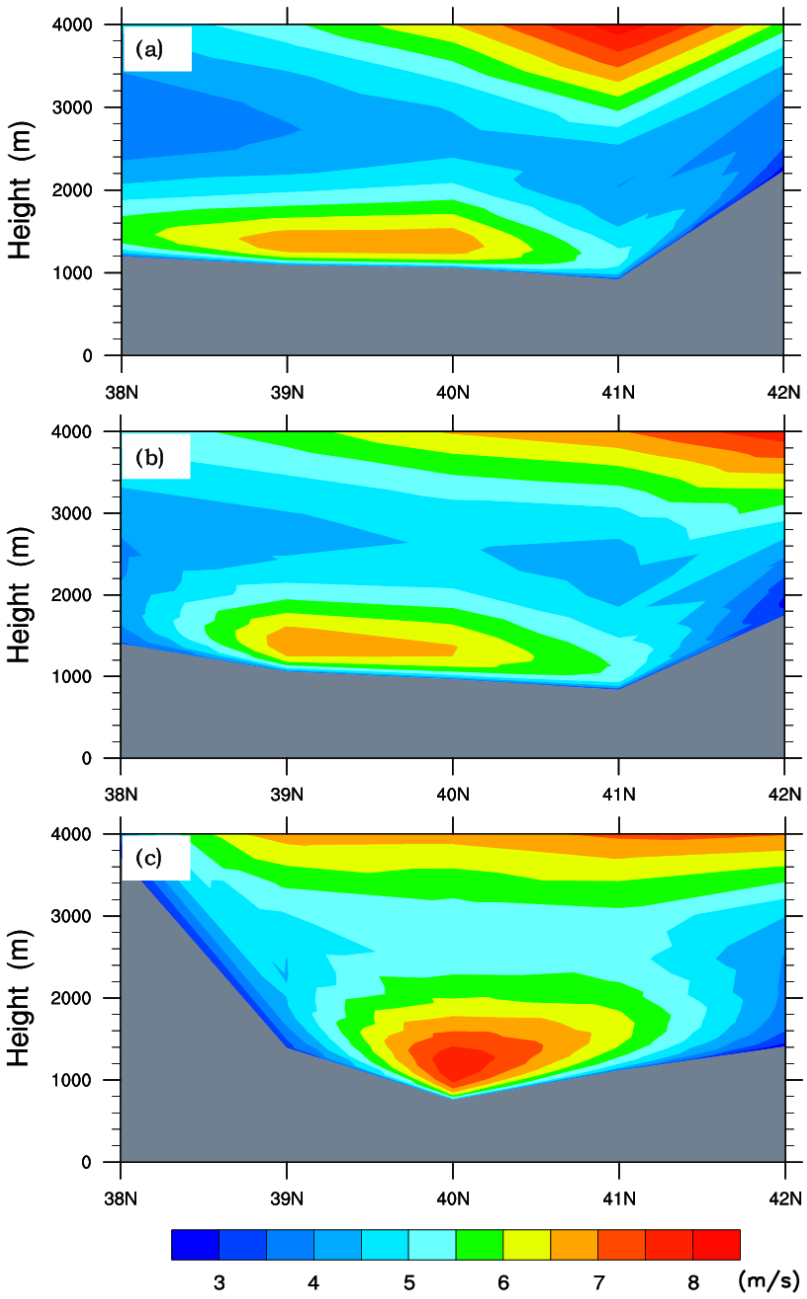

591

592 Figure 3. Latitude-height cross sections of annual mean wind speed at three

593 longitudes of (a) 82 ° E, (b) 85° E, and (c) 88 ° E from ERA-Interim reanalysis

594 averaged over 2000-2013. Gray areas represent the terrain elevation.

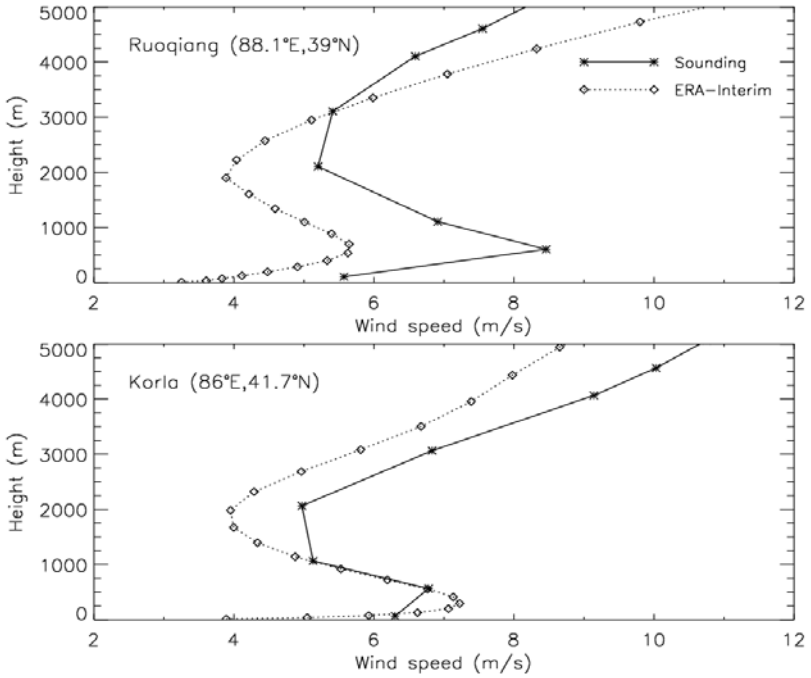

595

596 Figure 4. Mean wind speed profiles at 00 UTC based on radiosondes (solid line) and

597 ERA-Interim (dot line) at (a) Ruoqiang and (b) Korla sites for 2000 - 2012.

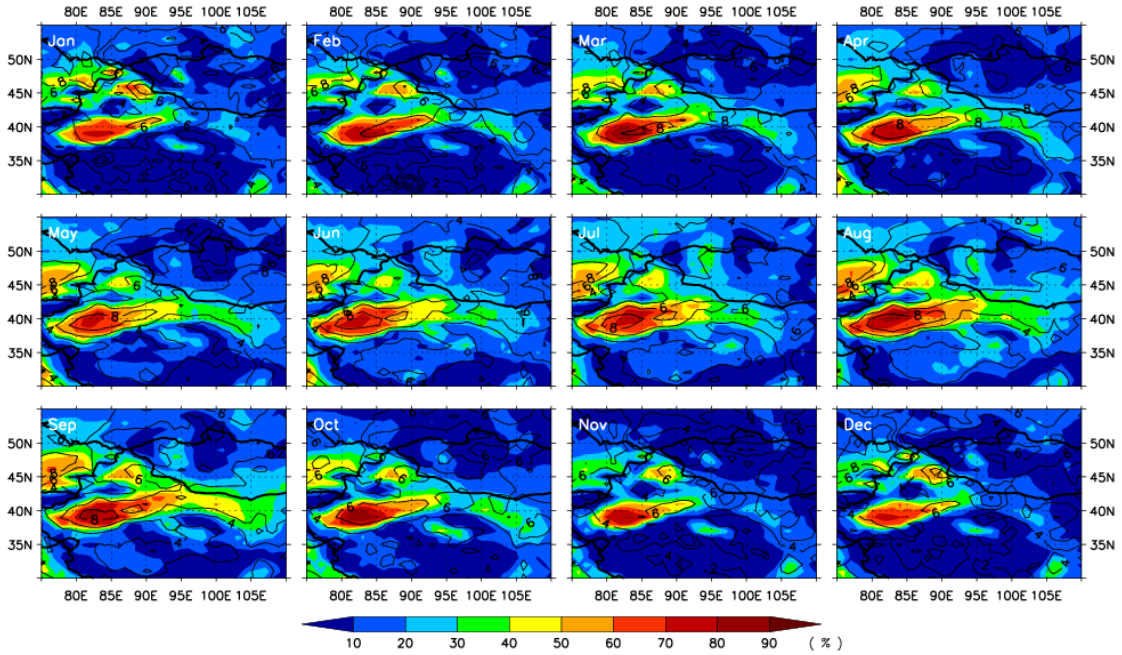

598

599 Figure 5. Monthly mean occurrence of NLLJs (colors) with jet core wind speed

600 (contours) at 00 UTC by applying the NLLJ detection algorithm to the ERA-Interim

601 reanalysis data for 2000-2013.

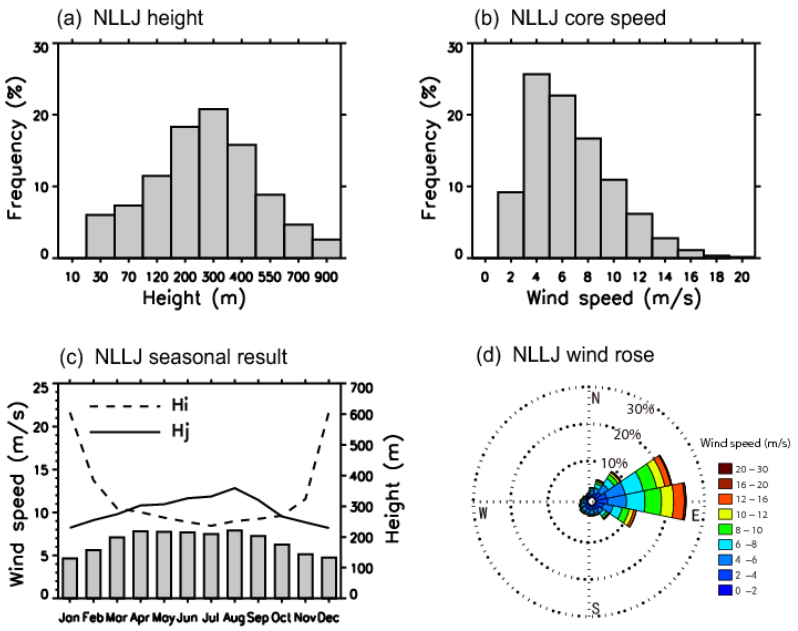

602

603 Figure 6. Climatological features of NLLJ over the Tarim Basin (38º-42º N, 78º-88º
604 E). (a) Frequency distribution of NLLJ height. (b) Frequency distribution of NLLJ
605 speed. (c) Monthly mean jet core speed (gray bar), NLLJ core height (solid line) and
606 inversion height (dashed line). (d) Jet core wind direction and speed distribution at 00
607 UTC (i.e., 0530 local) from ERA-Interim reanalysis from 2000 through 2013.

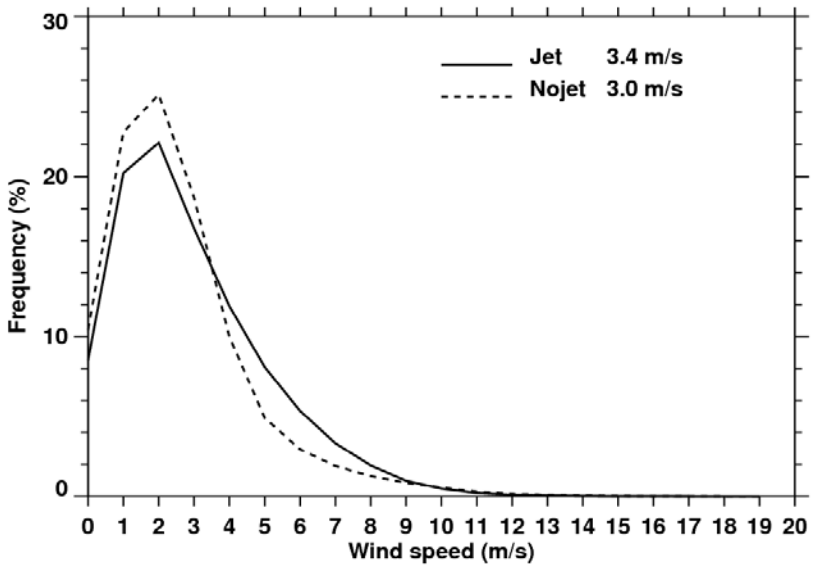

608

609 Figure 7. Frequency distribution of 10 m wind speed at 06 UTC (i.e. roughly at 1130

610 local time) over the Tarim basin.

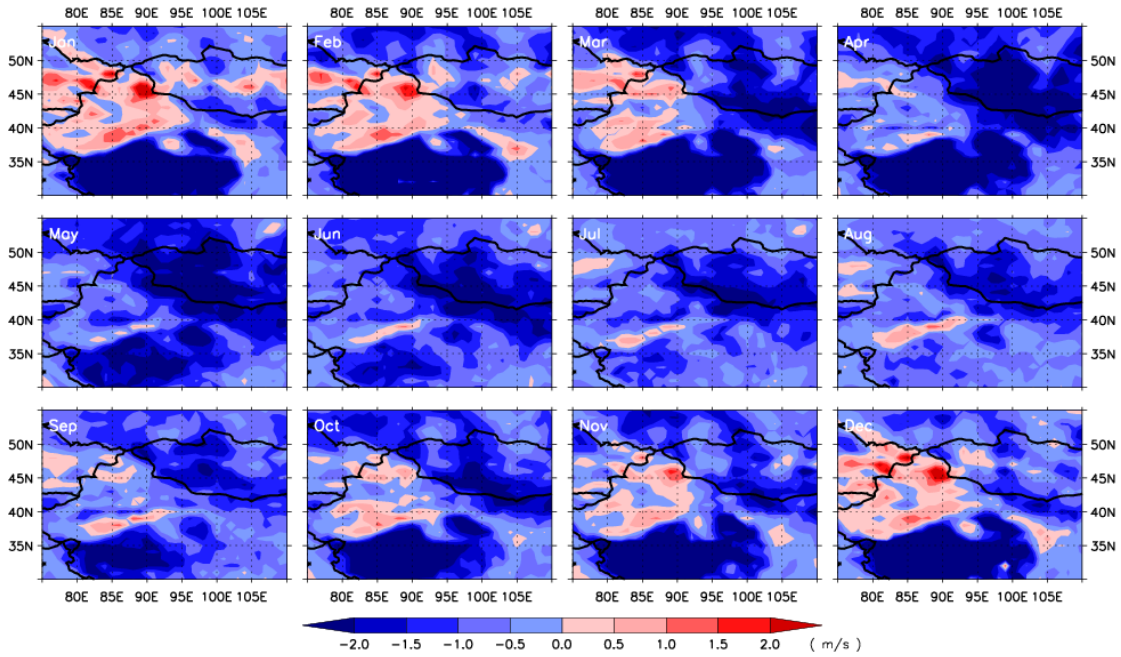

611

612 Figure 8. Annual cycle of the near surface wind speed difference at 06 UTC between

613 NLLJ and non-NLLJ days.

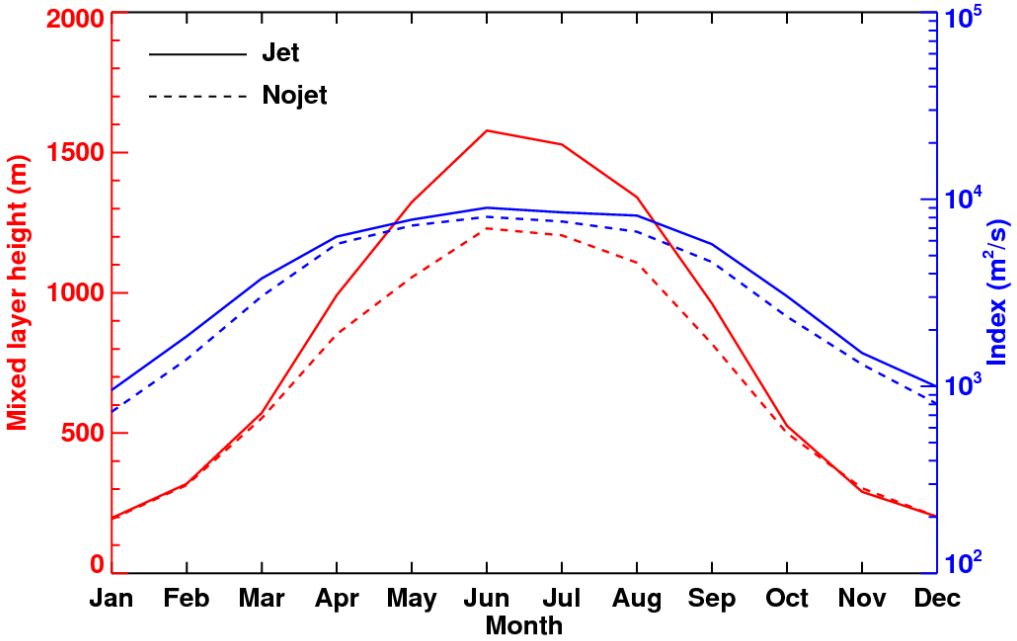

614

615 Figure 9. Monthly-averaged convection boundary layer height at 06 UTC, and

616 momentum index at 00 UTC over the TD.

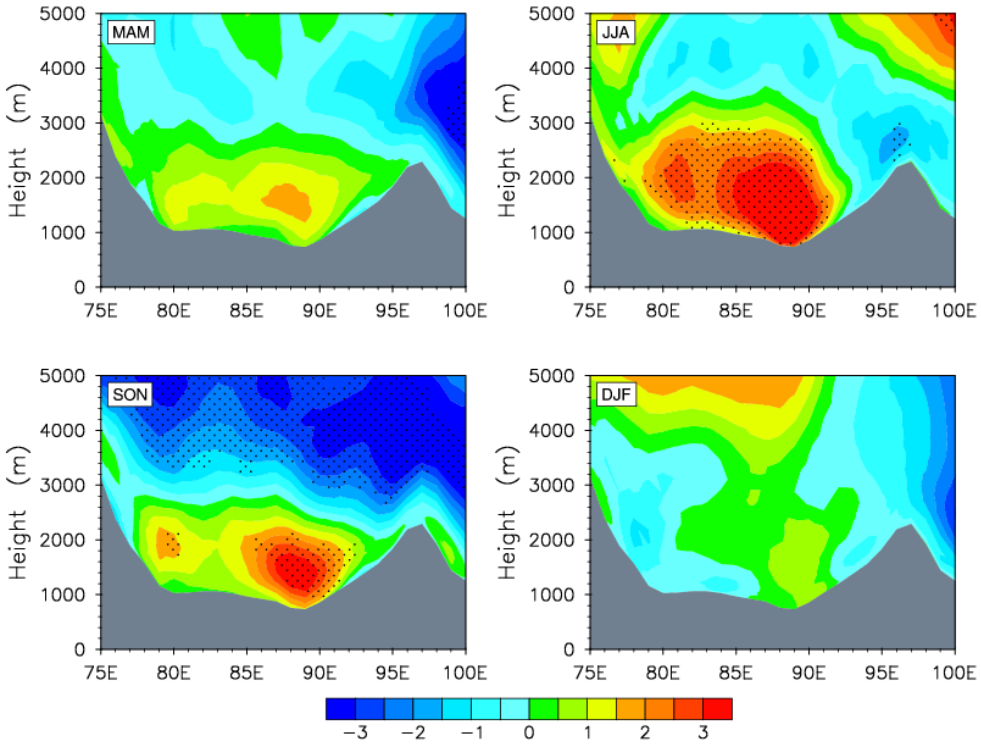

Figure 10. Seasonal longitudinal cross-sections of daily wind composite difference between high and low AOD days along 40º N. Stippled areas are significant at the 95% level. Gray areas represent terrain.